

Atrial natriuretic peptide regulates adipose tissue accumulation in adult atria

Nadine Suffee, Thomas Moore-Morris, Patrick Farahmand, Catherine Rucker-Martin, Gilles Dilanian, Magali Fradet, Daigo Sawaki, Genevieve Derumeaux, Pascal Leprince, Karine Clement, et al.

▶ **To cite this version:**

Nadine Suffee, Thomas Moore-Morris, Patrick Farahmand, Catherine Rucker-Martin, Gilles Dilanian, et al.. Atrial natriuretic peptide regulates adipose tissue accumulation in adult atria. Proceedings of the National Academy of Sciences of the United States of America, 2017, 114 (5), pp.E771-E780. 10.1073/pnas.1610968114 . hal-01785315

HAL Id: hal-01785315
https://amu.hal.science/hal-01785315

Submitted on 4 May 2018

HAL is a multi-disciplinary open access archive for the deposit and dissemination of scientific research documents, whether they are published or not. The documents may come from teaching and research institutions in France or abroad, or from public or private research centers.

L'archive ouverte pluridisciplinaire **HAL**, est destinée au dépôt et à la diffusion de documents scientifiques de niveau recherche, publiés ou non, émanant des établissements d'enseignement et de recherche français ou étrangers, des laboratoires publics ou privés.

CrossMark click for updates

Atrial natriuretic peptide regulates adipose tissue accumulation in adult atria

Nadine Suffee[a], Thomas Moore-Morris[b], Patrick Farahmand[c], Catherine Rücker-Martin[d], Gilles Dilanian[a], Magali Fradet[e], Daigo Sawaki[f], Geneviève Derumeaux[f], Pascal LePrince[a,c], Karine Clément[a,e], Isabelle Dugail[a], Michel Puceat[b], and Stéphane N. Hatem[a,e,1]

[a]Faculté de Médecine, Université Pierre et Marie Curie, Sorbonne University, INSERM UMR_S1166, Paris, France; [b]Faculté de Médecine La Timone, Université Aix-Marseille, INSERM UMR_910, Marseille, France; [c]Department of Cardiology, Pitié-Salpêtrière Hospital, Assistance Publique-Hôpitaux de Paris, Paris, France; [d]INSERM UMR_S999, Laboratory of Excellence in Research on Medication and Innovative Therapeutics, Institut Paris-Sud d'Innovation Thérapeutique Centre Chirurgical Marie Lanelongue, 92350 Le Plessis-Robinson, France; [e]Institute of Cardiometabolism and Nutrition, Paris, France; and [f]INSERM U_955, Département Hospitalo-Universitaire Ageing-Thorax-Vessels-Blood, Département de Physiologie, Hôpital Henri Mondor, Assistance Publique-Hôpitaux de Paris, Creteil, France

Edited by Christine E. Seidman, Howard Hughes Medical Institute, Harvard Medical School, Boston, MA, and approved December 13, 2016 (received for review July 6, 2016)

The abundance of epicardial adipose tissue (EAT) is associated with atrial fibrillation (AF), the most frequent cardiac arrhythmia. However, both the origin and the factors involved in EAT expansion are unknown. Here, we found that adult human atrial epicardial cells were highly adipogenic through an epithelial–mesenchymal transition both in vitro and in vivo. In a genetic lineage tracing the WT1$^{CreERT2+/-}$Rosa$^{tdT+/-}$ mouse model subjected to a high-fat diet, adipocytes of atrial EAT derived from a subset of epicardial progenitors. Atrial myocardium secretome induces the adipogenic differentiation of adult mesenchymal epicardium-derived cells by modulating the balance between mesenchymal Wingless-type Mouse Mammary Tumor Virus integration site family, member 10B (Wnt10b)/β-catenin and adipogenic ERK/MAPK signaling pathways. The adipogenic property of the atrial secretome was enhanced in AF patients. The atrial natriuretic peptide secreted by atrial myocytes is a major adipogenic factor operating at a low concentration by binding to its natriuretic peptide receptor A (NPRA) receptor and, in turn, by activating a cGMP-dependent pathway. Hence, our data indicate cross-talk between EAT expansion and mechanical function of the atrial myocardium.

epicardial adipose tissue | epicardial progenitors | atrial natriuretic peptide | cGMP

The adipose tissue (AT) that accumulates at the surface and underneath the epicardium, referred as to "epicardial adipose tissue" (EAT), is a common histological component of the atrial myocardium. Anatomically, EAT is considered to be a specific visceral AT depot responsible for the local delivery of fatty acid and adipokine substrates that can freely diffuse into the neighboring myocardium (1). However, the recognition that EAT can be associated with the risk and severity of atrial fibrillation (AF), the most frequent cardiac arrhythmia in clinical practice, suggests that this visceral fat tissue is not always harmless or beneficial (2–4). For instance, EAT can promote fibrosis of the neighboring atrial myocardium, the substrate of AF, by secreting cytokines such as Activin A (5) or by favoring fibrosis of the atrial subepicardium (6). Therefore understanding the origin of atrial EAT and identifying the factors regulating its local development is of major interest.

The outer mesothelial layer of the heart, the epicardium, contains a number of multipotent progenitor cells that can undergo an epithelial-to-mesenchymal transition (EMT) process, giving rise to multipotent mesenchymal epicardium-derived cells (EPDCs) (7–10). Recently it has been shown that epicardial-derived cells differentiate into adipocytes during early postnatal development, contributing to physiological fat or EAT accumulation in the atrial–ventricular groove (10). Whether this epicardial-to-fat transition can occur in the adult heart is being actively investigated. In adult mice overexpressing the adipogenic transcriptional factor peroxisome proliferator-activated receptor-γ (PPARγ) and after massive acute myocardial injury, some adipocytes derived from the epicardium were detected in the ventricle (10, 11). Protein factors such as Insulin-like growth factor 1 receptor (IGF1R) govern the formation of ventricular EAT after acute myocardial infarction (12).

Here we provide evidence that atrial EAT derives from adult atrial epicardial cells via EMT. Furthermore, we reveal that a low dose of atrial natriuretic peptide (ANP) secreted by atrial myocytes promotes adipogenic differentiation of adult EPDCs (aEPDCs) by binding to the NPRA type receptor and activating cGMP signaling. This ANP-mediated cross-talk between the myocardium and the epicardium reveals a link between EAT expansion and the mechanical properties of the atrial myocardium.

Results

Adult Atrial Epicardium Is Adipogenic. Because EAT is closely associated with the epicardium, we first investigated whether human atrial epicardium contained adipocyte progenitors (Table S1). In the epicardial area of human atria, where AT depots were commonly observed (Fig. 1 *A* and *B*), some cells expressed Wilm's tumor 1 (WT1) and Insulin gene enhancer protein 1 (Islet-1), respectively, two markers of epicardial and myocardial progenitors (Fig. 1 *C* and *D*) (7, 13, 14). However, there was no clear relationship between the presence of these progenitor cells and the clinical history of donors (Table S1). In the epicardial layer, some WT1$^+$ and Islet-1$^+$ cells also expressed mesenchymal markers such as the cytoskeleton proteins vimentin and α-smooth muscle actin (α-SMA), suggesting that they might have been derived from EMT of the adult

Significance

Atrial fibrillation is the most frequent cardiac arrhythmia and is a major cause of stroke. Recently, it has been shown that the adipose tissue that accumulates at the surface of the heart contributes to the pathogenesis of atrial fibrillation by favoring fibrosis of the neighboring myocardium. However, the cellular origin of adult cardiac fat tissue is unknown. Here, we show that resident progenitor cells of the external layer of the heart, referred to as the "epicardium," are a source of adipocytes through an epithelial-to-mesenchymal transition process. The atrial natriuretic peptide, which is secreted by atrial myocytes, is a potent factor in the differentiation of epicardial progenitors in adipocytes. Our data uncover cross-talk between myocardial mechanical properties and adipose tissue expansion.

Author contributions: N.S., T.M.-M., I.D., M.P., and S.N.H. designed research; N.S., T.M.-M., P.F., C.R.-M., G. Dilanian, M.F., and D.S. performed research; N.S. and T.M.-M. contributed new reagents/analytic tools; N.S., T.M.-M., P.F., C.R.-M., G. Dilanian, M.F., D.S., G. Derumeaux, P.L., K.C., I.D., M.P., and S.N.H. analyzed data; and N.S., T.M.-M., G. Derumeaux, P.L., I.D., M.P., and S.N.H. wrote the paper.

The authors declare no conflict of interest.

This article is a PNAS Direct Submission.

[1]To whom correspondence should be addressed. Email: stephane.hatem@upmc.fr.

This article contains supporting information online at www.pnas.org/lookup/suppl/doi:10.1073/pnas.1610968114/-/DCSupplemental.

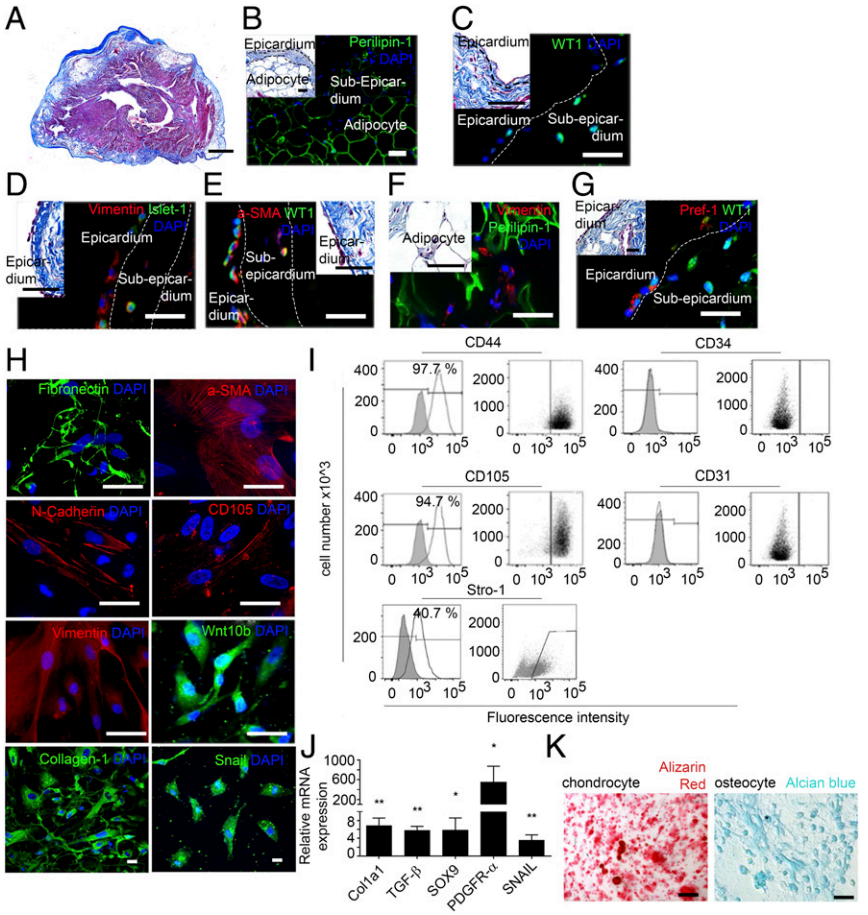


Fig. 1. Human atrial epicardial progenitor cells have mesenchymal properties. (*A*) Masson's trichrome staining of 7-μm-thick sections of human atrial tissue ($n = 26$). (Scale bar, 100 μm.) (*B*–*G*) Immunofluorescence staining in human atrial tissue sections ($n = 8$) for Perilipin-1 (*B*), WT1 (*C*), vimentin and Islet-1 (*D*), α-SMA and WT1 (*E*), vimentin and Perilipin-1 (*F*), and Pref-1 and WT1 (*G*). (Scale bars, 20 μm.) *Insets* show Masson's trichrome staining. (Scale bars, 10 μm.) (*H*) Immunofluorescence staining of aEPDCs for fibronectin, α-SMA, N-cadherin, CD105, vimentin, Wnt10b, collagen-1, Snail, and DAPI ($n = 10$). (Scale bars, 10 μm.) (*I*) Flow cytometry of aEPDCs for CD44, CD105, CD31, CD34, and Stro-1 markers ($n = 10$). Specific isotype controls are shown in gray. (*J*) Quantitative PCR (qPCR) analysis for Col1a1, TGFβ, SOX9, PDGFRα, and SNAIL in aEPDCs. Data are expressed as the fold change relative to unpassaged aEPDCs ($n = 15$) and represent the mean ± SEM of independent experiments. $^*P < 0.05$, $^{**}P < 0.01$, one-way ANOVA and Bonferroni's post hoc test. (*K*) Bright-field images of aEPDC-derived chondrocytes or osteocytes revealed by alizarin red or Alcian blue staining, respectively ($n = 3$). (Scale bars, 20 μm.)

epicardium and had migrated outside the epicardial layer (Fig. 1 *D* and *E*) (15). Vimentin-positive cells also were seen in the vicinity of mature adipocytes in subepicardium (Fig. 1*F*). $WT1^+$ cells coexpressing the preadipocyte factor 1 (Pref-1, encoded by the gene *DLK1*) were present in the epicardium (Fig. 1*G*). They could represent resident preadipocytes, in keeping with the observation of a number of $WT1^+$/$Pref\text{-}1^+$ cells in the epicardium of atria of embryonic mice (Fig. S1).

Next, we investigated the adipogenic capacity of atrial aEPDCs by harvesting and culturing epicardial cells from samples of human right atria obtained from 35 patients undergoing cardiac surgery (Table S1). After 2 d in culture, primary epicardial cells migrated out of the explants and showed the characteristics typical of epicardial progenitors including squamous morphology and the expression of epicardial progenitor markers such as WT1, Transcription factor 21 (TCF21), and Connexin-43 (Fig. S2*A*). They expressed high levels of *WT1* and T-box transcription factor 18 (*TBX18*) (another epicardium progenitor marker) transcripts compared with cardiac myocytes (Fig. S2*B*). After the first passage and until passages 5–6, primary cells spontaneously acquired and retained a mesenchymal stem cell (MSC) morphology and expressed several mesenchymal proteins, including matrix proteins such as fibronectin and collagen-1, the cytoskeleton proteins α-SMA, vimentin, Wingless-type Mouse Mammary Tumor Virus integration site family, member 10B (Wnt10b), the membrane protein N-cadherin, CD105, and the nuclear protein Snail (Fig. 1*H*). Mesenchymal proteins such as CD44, CD105, and the cell surface antigen Stro-1, but not the endothelial markers CD31 and CD34, were present at the plasma membrane of aEPDCs as evidenced by flow cytometry (Fig. 1*I*). The mesenchymal transition of primary epicardial cells also was supported by the expression of EMT-related genes, including Snail family transcriptional repressor (*SNAIL*) (Fig. 1*J*) (7, 16). Finally, confirming their mesenchymal characteristics, we found that aEPDCs had an osteogenic and chondrogenic potential equivalent to that of human MSCs (Fig. 1*K* and Fig. S3) (17).

We next examined the adipogenic capacity of aEPDCs by using two distinct culture media known to induce massive adipogenic differentiation of human MSCs (17, 18). Indeed, after 21 d, a subset of aEPDCs showed lipid accumulation as revealed by Oil Red O staining (Fig. 2 *A* and *B*). In addition, both proteins and mRNA transcripts encoding *Adipokine*, *Perilipin-1*, *CCAAT/Enhancer binding protein-α* (*C/EBPα*), and *PPARγ*, the two last genes being master transcriptional regulators of adipocyte differentiation (10, 16, 19), were induced in aEPDCs (Fig. 2 *C*–*E*) (Table S2). Between days 7 and 30 of culture in adipogenic medium, flow cytometry revealed Pref-1 down-regulation and Perilipin-1 up-regulation in aEPDCs, indicating a shift from pre- to mature adipocytes (Fig. 2*F*). Of note, there was marked heterogeneity in the percentage of adipocytes (from 0 to 95%) derived from aEPDCs of the different donors. Furthermore, aging was associated with a high adipogenic capacity of aEPDCs ($r^2 = 0.24$, $P = 0.027$), whereas left ventricular dysfunction (ejection fraction <45%) was associated with reduced adipogenic capacity ($r^2 = 0.21$, $P = 0.046$).

Next we examined the epicardial contribution to EAT formation in situ. We first defined the optimal conditions for reproducing EAT accumulation in mouse hearts. We examined whether obesity induced by a high-fat diet (HFD) could be associated with atrial fat deposition. We found that the left atria of adult C57BL/6 mice maintained on an obesogenic HFD for a prolonged period exhibited a clear EAT accumulation, mainly in the epicardial layer, which we did not observe in mice fed a normal diet (Fig. 3 *A* and *B*). Although we did not first observe subepicardial fat, as seen in human patients, after 4 months cells coexpressing WT1 and Pref-1 were detected both at the pericardial and myocardial faces of the sup-epicardium of obese

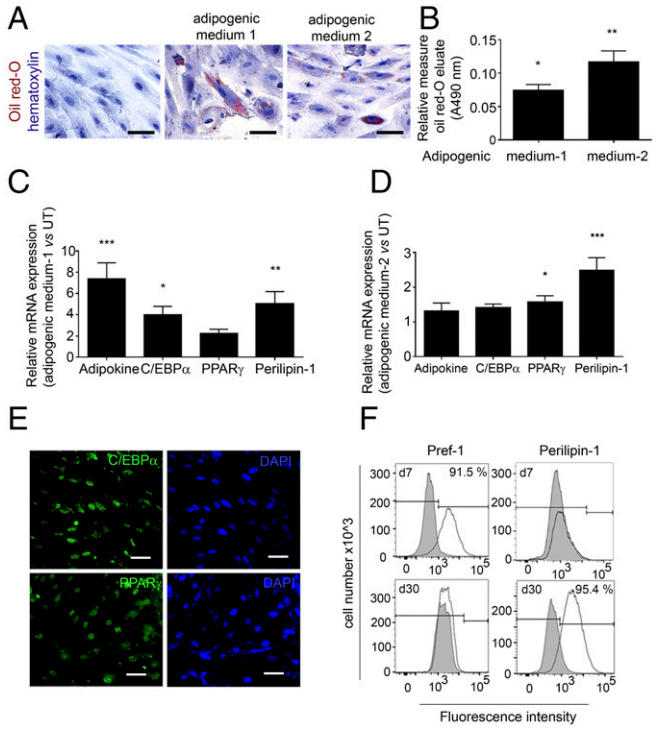


Fig. 2. Human EPDCs have the capacity to differentiate into adipocytes in vitro. (*A*) Bright-field images of aEPDCs treated with adipogenic medium 1 or medium 2 or with basal medium stained with Oil Red O to identify lipid droplet formation and counterstained with hematoxylin ($n = 35$). (Scale bars, 20 μm.) (*B*) Histogram showing Oil Red O content (A490) ($n = 35$). Data represent values relative to untreated aEPDCs and are expressed as mean ± SEM of independent experiments, $*P < 0.05$, $**P < 0.01$, one-way ANOVA and Bonferroni's post hoc test. (*C* and *D*) Expression of adipokine, C/EBPα, PPARγ, and Perilipin-1 in aEPDCs treated with adipogenic medium 1 (*C*) or medium 2 (*D*) ($n = 10$). Data represent the fold change relative to untreated aEPDCs and are expressed as the mean ± SEM of independent experiments. $*P < 0.05$, $**P < 0.01$, $***P < 0.001$, one-way ANOVA and Bonferroni's post hoc test. (*E*) Immunofluorescence staining for C/EBPα and PPARγ in aEPDCs treated with adipogenic medium 1. (Scale bars, 20 μm.) (*F*) Histograms show aEPDC Pref-1 and Perilipin-1 signal intensity analyzed by flow cytometry following treatment with adipogenic medium 2 for 7 or 30 d ($n = 6$). Isotype controls are shown in gray.

mice fed an HFD (Fig. 3*B*). Furthermore, the expression of adipocyte gene markers was up-regulated in atria (Fig. 3*C*). Although the mice fed an HFD showed no evidence of cardiopathy on echocardiography imaging, they were more susceptible to AF than lean animals, as indicated by the increased percentage of mice that developed AF in response to burst pacing and by a longer duration of AF episodes (Fig. S4).

To establish whether adult epicardium is adipogenic in vivo, we performed genetic lineage tracing of adult epicardial cells in $WT1^{CreERT2+/-}Rosa^{tdT+/-}$ mice subjected to the adipogenic nutritional protocol described above. Adult epicardial cells were specifically and irreversibly labeled following tamoxifen induction in young adults. The HFD-induced EAT deposition was reproduced successfully in $WT1^{CreERT2+/-}Rosa^{tdT+/-}$ adult mice, which accumulated AT in the sup-epicardium after 4 mo of HFD (Fig. 3*D*). In mice subjected to HFD, but not in control mice fed a normal diet, we observed tandem dimer Tomato (tdT^+) aEPDCs in the left atrial sup-epicardium. Furthermore, a subset of these tdT^+ aEPDCs coexpressed the adipocyte marker Perilipin-1, suggesting that they were adipocytes derived directly from adult epicardium (Fig. 3*E*). Expression of PPARγ also was observed in tdT^+ cells that exhibited fully mature adipocyte morphology within the epicardial adipose layer (Fig. 3*F*).

Next, to establish the adipogenic potential of mouse atrial epicardium, epicardial cells were harvested from $WT1^{CreERT2+/-}Rosa^{tdT+/-}$ atria as described for human epicardium. At day 1, tdT^+ cells migrated from atrial tissue onto the culture dish, showed typical squamous morphology (Fig. 3*G*), and expressed the nuclear marker TCF21 attesting their epicardial origin (Fig. 3*H*) (20). These tdT^+ cells underwent EMT spontaneously, acquiring a mesenchymal morphology as observed at day 3 (Fig. 3*G*). The mesenchymal transition was confirmed by the up-regulation of matrix (collagen-1), cytoskeleton (α-SMA, vimentin), and membrane (CD90/thymus cell antigen-1) proteins, as well as the nuclear marker Snail (Fig. 3*H*). From the second passage, tdT^+ murine aEPDCs exposed to adipogenic medium for 21 d showed lipid droplet accumulation, indicating they had undergone adipogenic differentiation (Fig. 3 *I* and *J*). Taken together, these results indicate that during obesity-induced EAT accumulation, epicardial progenitors undergo EMT and contribute directly to adipocyte accumulation.

Atrial Myocardium Secretes Adipogenic Factors. A previous study reporting that atrial myocardium can secrete adipogenic factors (21) prompted us to examine the impact of either EAT or myocardial (MYO) secretomes (-S), derived from patient explants (Table S1) on human aEPDCs in culture. Between days 7 and 30, MYO-S but not EAT-S induced a shift from Pref-1^+ preadipocytes to mature adipocytes containing Oil Red-O–stained lipid droplets and expressing Perilipin-1 (Fig. 4 *A*–*D* and *F*), PPARγ, and C/EBPα (Fig. 4 *C*, *D*, and *F*). There was significant variability in the adipogenic effect of atrial secretomes. Compared with secretomes from patients without AF, atrial secretomes from AF patients had a more pronounced adipogenic capacity on both aEPDCs and MSCs (Fig. S5).

We next examined the kinases involved in aEPDC adipogenesis. After 24 h of culture in the presence of MYO-S, the promesenchymal Wnt/β-catenin/Glycogen synthase kinase 3 (GSK-3β) and Stress-activated protein kinase (SAPK)/JNK MAPK signaling pathways (22, 23) were suppressed (Fig. 4*E*). These results were in agreement with the observation of the suppression of mesenchymal genes Collagen 1α (*Col1a1*), *SNAIL*, Sex-determining region box 9 (*SOX9*), and *TGFβ* and the parallel expression of adipogenic genes by aEPDCs stimulated with MYO-S for 21 d (Fig. 4*F*). Next, we found that ERK/MAPK and PI3K/AKT, which are part of the adipogenic signaling pathways (22, 23), remained activated in aEPDCs (Fig. 4*G*). In contrast, PD98059 and U0126, specific antagonists of ERK/MAPK and ERK2, respectively (19, 22, 23), suppressed the expression of C/EBPα and decreased the expression of PPARγ induced by MYO-S (Fig. 4*H*). Of note, neither antagonist had an effect on untreated aEPDCs. These results indicate that MYO-S contains adipogenic factors that specifically regulate signaling pathways governing epicardial cell fate.

ANP Mediates the Adipogenic Effects of Atrial Myocardial Secretome Through cGMP Signaling. Using a protein screening assay, we found that a number of growth factors, cytokines, and metalloproteases were present in both EAT-S and MYO-S (Fig. S6). However, only FGF-7, Bone morphogenic protein 4 (BMP-4), and ANP were detected exclusively in MYO-S (Fig. 5 *A* and *B*). First, we tested the soluble proteins FGF-7 and BMP-4, which did not induce adipogenesis of aEPDCs (24). Second, the involvement of ANP in the adipogenic effect of MYO-S was tested first by culturing human aEPDCs in the presence of increasing concentrations (1, 10, 100, and 10 000 pM) of human recombinant ANP. After 21 d in culture, 62 ± 0.3% of cells incubated with 10 pM of ANP contained lipid droplets stained with Oil Red O (Fig. 5*C*) and expressed Perilipin-1 (Fig. 5*D*). Higher concentrations of human recombinant ANP (1 and 10 nM) did not further increase the percentage of aEPDC-derived adipocytes but instead reduced cell lipid content, suggesting a lipolytic effect (Fig. 5 *C* and *D*). Of note, the adipogenic effect of ANP was observed in the range of the peptide concentration found in

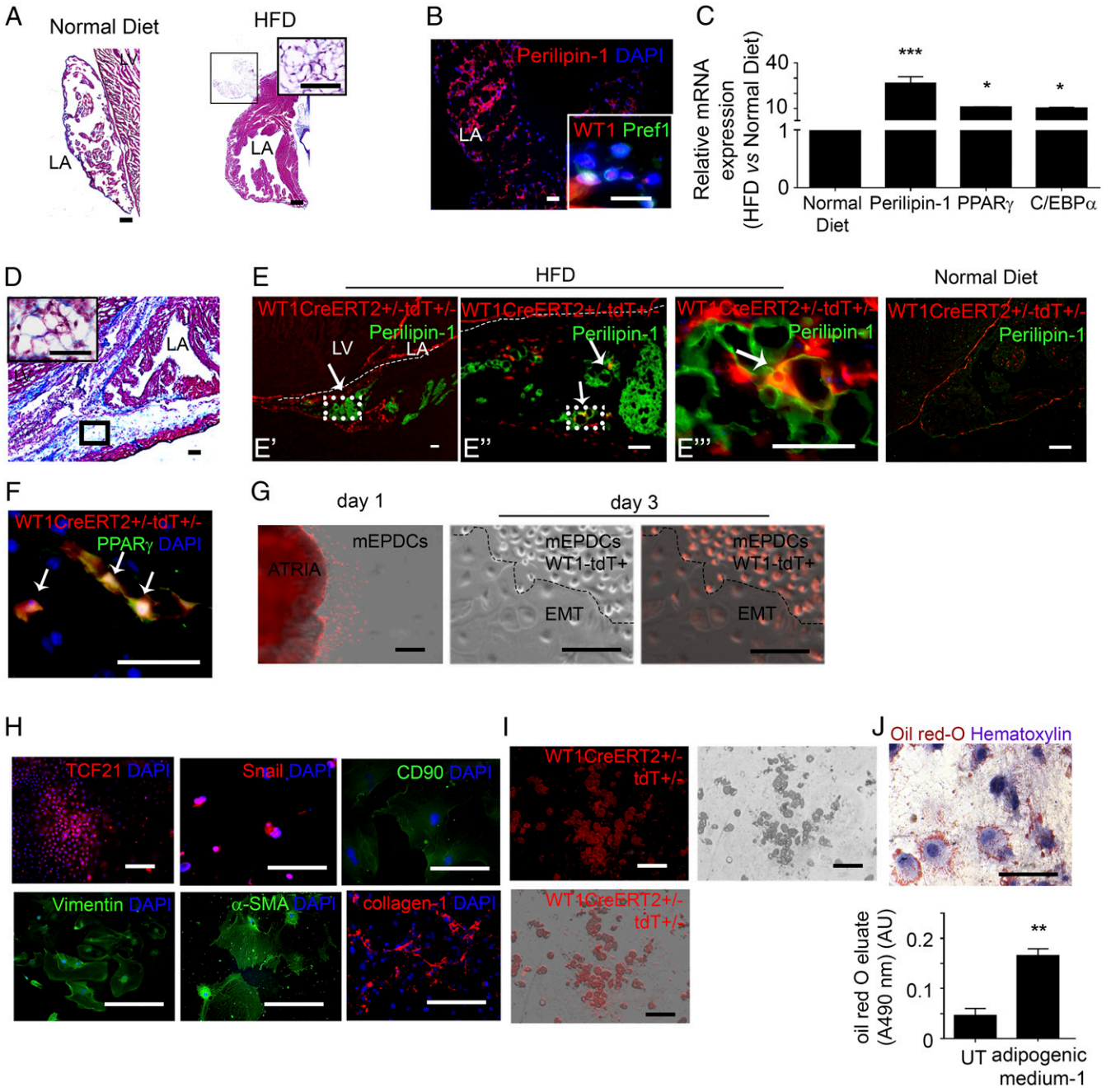


Fig. 3. Obesity induces atrial epicardium-to-fat transition in mice. (*A* and *D*) Masson's trichrome staining of 7-μm-thick sections of left atrial tissue (LA) in control mice ($n = 10$) (*A*) and WT1CreERT2$^{+/-}$;tdT$^{+/-}$ mice ($n = 8$) (*D*), both fed an HFD. (Scale bar: 60 μm in *A*, 20 μm in *D*, 10 μm in *Insets*). (*B*) Immunofluorescence staining for Perilipin-1 in mice fed an HFD ($n = 5$), Pref-1 and WT1 (*Inset*) in mice fed a normal diet ($n = 5$). (Scale bars, 10 μm.) (*C*) qPCR analysis of Perilipin-1, PPARγ, and C/EBPα expression in control mice fed a normal diet ($n = 5$). Data are represented as the fold change in mice fed an HFD relative to mice fed a normal diet and are expressed as the mean ± SEM of five independent experiments, $^{*}P < 0.05$, $^{***}P < 0.001$, one-way ANOVA and Bonferroni's post hoc test. (*E* and *F*) Immunostaining for Perilipin-1 (*E*) or PPARγ (*F*) in atria of WT1CreERT2$^{+/-}$;tdT$^{+/-}$ mice fed an HFD ($n = 8$). Arrows indicate signal colocalization in each enlargement (*E'*, *E''*, and *E'''*) of epicardium-derived adipocytes. (Scale bars, 20 μm.) (*G*) Overlapped phase-contrast and fluorescence images of aEPDCs migrating from a WT1CreERT2$^{+/-}$; tdT$^{+/-}$ atrial explant at day 1 and day 3 in culture ($n = 5$). (Scale bars, 200 μm.) (*H*) WT1CreERT2$^{+/-}$;tdT$^{+/-}$ aEPDCs immunostained for TCF21, Snail, CD90, vimentin, α-SMA, and collagen-1 ($n = 5$). (Scale bars, 50 μm.) (*I* and *J*) Bright-field, fluorescence, and overlapped fields (*I*) and Oil Red O/hematoxylin staining (*J*) of WT1CreERT2$^{+/-}$;tdT$^{+/-}$ aEPDCs induced by adipogenic medium 1 for 21 d ($n = 5$). (Scale bars, 200 μm.) The histogram in *J* represents Oil Red O elution A490 compared with untreated aEPDCs ($n = 5$). Data are expressed as the mean ± SEM of five independent experiments. $^{**}P < 0.01$, one-way ANOVA and Bonferroni's post hoc test. AU, arbitrary units; LA, left atria; LV, left ventricle; UT, untreated.

MYO-S (25, 26). Screening the supernatant of adipocytes derived from aEPDCs revealed a number of proteins belonging to the inflammatory protein family (TNF-α and interleukins) involved in extracellular matrix turnover [tissue inhibitor of metalloproteinase 1 and 2 (TIMP-1 and -2)] or expressed by mature adipocytes [BMP-4, Pre-B-cell–enhancing factor-related protein (PBEF), leptin, and Pref-1] (Fig. S7) (27, 28).

ANP regulates the balance between the cGMP and cAMP signaling pathways (29–31) that was examined using two permeant analogs of cyclic nucleotides, 8-Bromo-cGMP (8-Br-cGMP) and

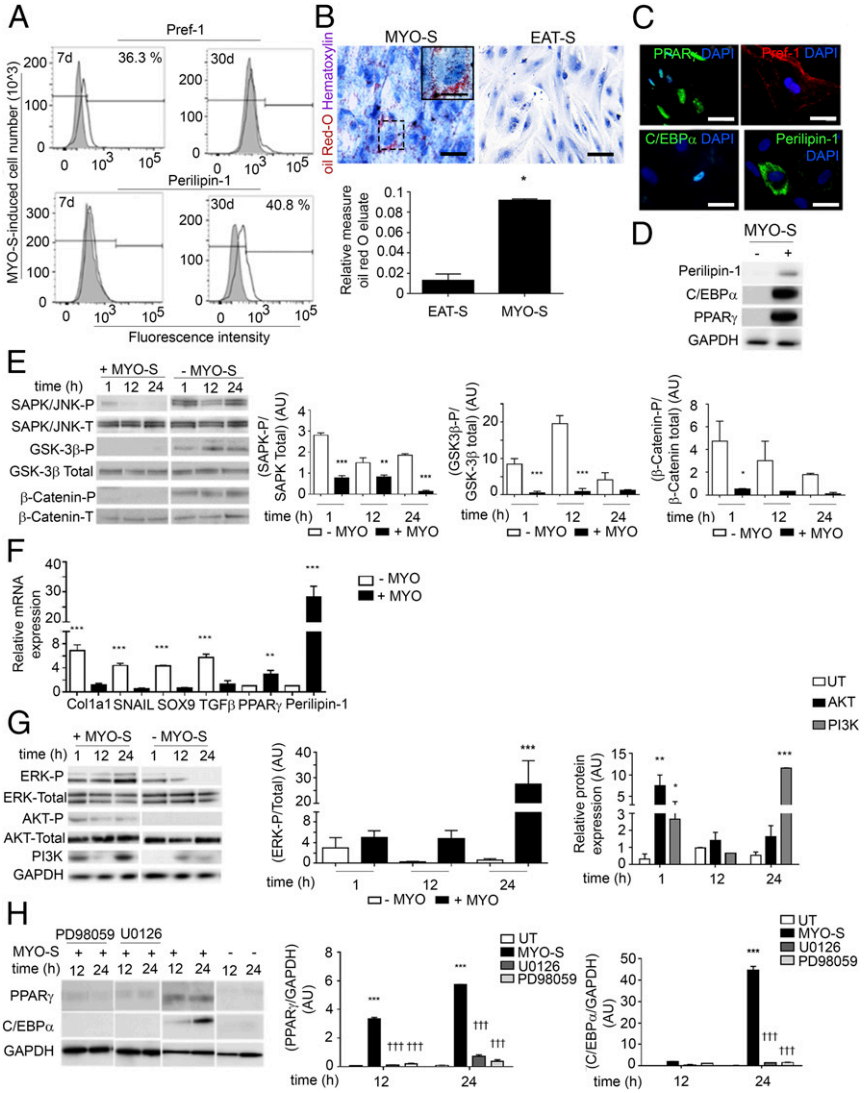


Fig. 4. The secretome of human atria is a potent inducer of EMT and adipogenic differentiation of epicardial cells. (*A*) Flow cytometry analysis for Pref-1 and Perilipin in aEPDCs treated with MYO-S for 7 or 30 d ($n = 10$). (*B*) Representative images of aEPDCs incubated with MYO-S or EAT-S stained with Oil Red O and counterstained with hematoxylin ($n = 10$). (Scale bars: 20 μm; *Inset* 5 μm.) The histogram represents the relative level of Oil Red O staining in treated vs. untreated cells. Data are expressed as the mean ± SEM of independent experiments. $^{*}P < 0.05$, one-way ANOVA and Bonferroni's post hoc test. (*C*) Immunostaining for PPARγ, Pref-1, C/EBPα, and Perilipin-1 of aEPDCs treated with MYO-S ($n = 10$). (Scale bars, 10 μm.) (*D*) Immunoblot analysis of Perilipin-1, C/EBPα, and PPARγ in aEPDCs treated with MYO-S for 21 d ($n = 3$). (*E* and *G*) Immunoblots and relative quantification of SAPK/JNK, GSK-3β, and β-catenin (*E*) and ERK1/2, AKT, and PI3K (*G*) signaling pathways in aEPDCs treated with MYO-S for 1, 12, or 24 h compared with untreated cells ($n = 3$). Data are expressed as the mean ± SEM of three independent experiments. $^{*}P < 0.05$, $^{**}P < 0.01$, $^{***}P < 0.001$, one-way ANOVA and Bonferroni's post hoc test. (*F*) qPCR analysis for Col1a1, SNAIL, SOX9, TGFβ, PPARγ, and Perilipin-1 in aEPDCs treated with MYO-S ($n = 5$). Data are presented as the fold change relative to untreated aEPDCs and are expressed as the mean ± SEM of independent experiments. $^{**}P < 0.01$, $^{***}P < 0.001$, one-way ANOVA and Bonferroni's post hoc test. (*H*) Immunoblots and relative quantification for PPARγ and C/EBPα expression in aEPDCs pretreated with PD98059 or U0126 and stimulated with MYO-S for 12 or 24 h ($n = 3$). Data are expressed as the mean ± SEM of independent experiments. $^{***}P < 0.001$ compared with untreated aEPDCs; $^{\dagger\dagger\dagger}P < 0.001$ compared with MYO-S; one-way ANOVA and Bonferroni's post hoc test.

8-Bromo-cAMP (8-Br-cAMP) (32). Only the former induced the accumulation of lipid droplets as well as C/EPBα and Perilipin-1 expression in aEPDCs (Fig. 5*E*). Furthermore, it induced several adipogenic genes such as *Adipokine*, *PPARγ*, *C/EBPα*, and *Perilipin-1* while reducing the expression of mesenchymal transcripts (Fig. 5*F*). Low ANP concentrations that induced adipogenic differentiation of aEPDCs were associated with the activation of cGMP-dependent protein kinase (PKG) pathways, whereas higher concentrations of the peptide induced lipolysis and activated cAMP-dependent protein kinase (PKA) pathways (Fig. 5*G*). Additional evidence that the adipogenic effect of ANP involved cGMP-dependent pathways came from the observation of decreased expression of transcription factors C/EBPα and PPARγ in aEPDCs treated with the cGMP antagonist Rp-cGMP (Rp-8-bromo-β-phenyl-1,N2-ethenoguanosine 3′,5′-cyclic monophosphorothioate sodium) (Fig. 5*H*). Similar inhibition of C/EBPα and PPARγ expression also was observed in cells treated with ANP and the nonspecific phosphodiesterase (PDE) inhibitor W7 [*N*-(6-Aminohexyl)-5-chloro-1-naphthalenesulfonamide hydrochloride] (Fig. 5*H*). Finally, cells treated with Rp-cGMP and W7 maintained their mesenchymal state through β-catenin signaling pathway phosphorylation (Fig. 5*I*).

ANP binds to natriuretic peptide receptors (NPR) A, B, and C, the last being a clearance receptor (33). In the heart, NPRA acts as a particular type of guanylyl cyclase (33). In

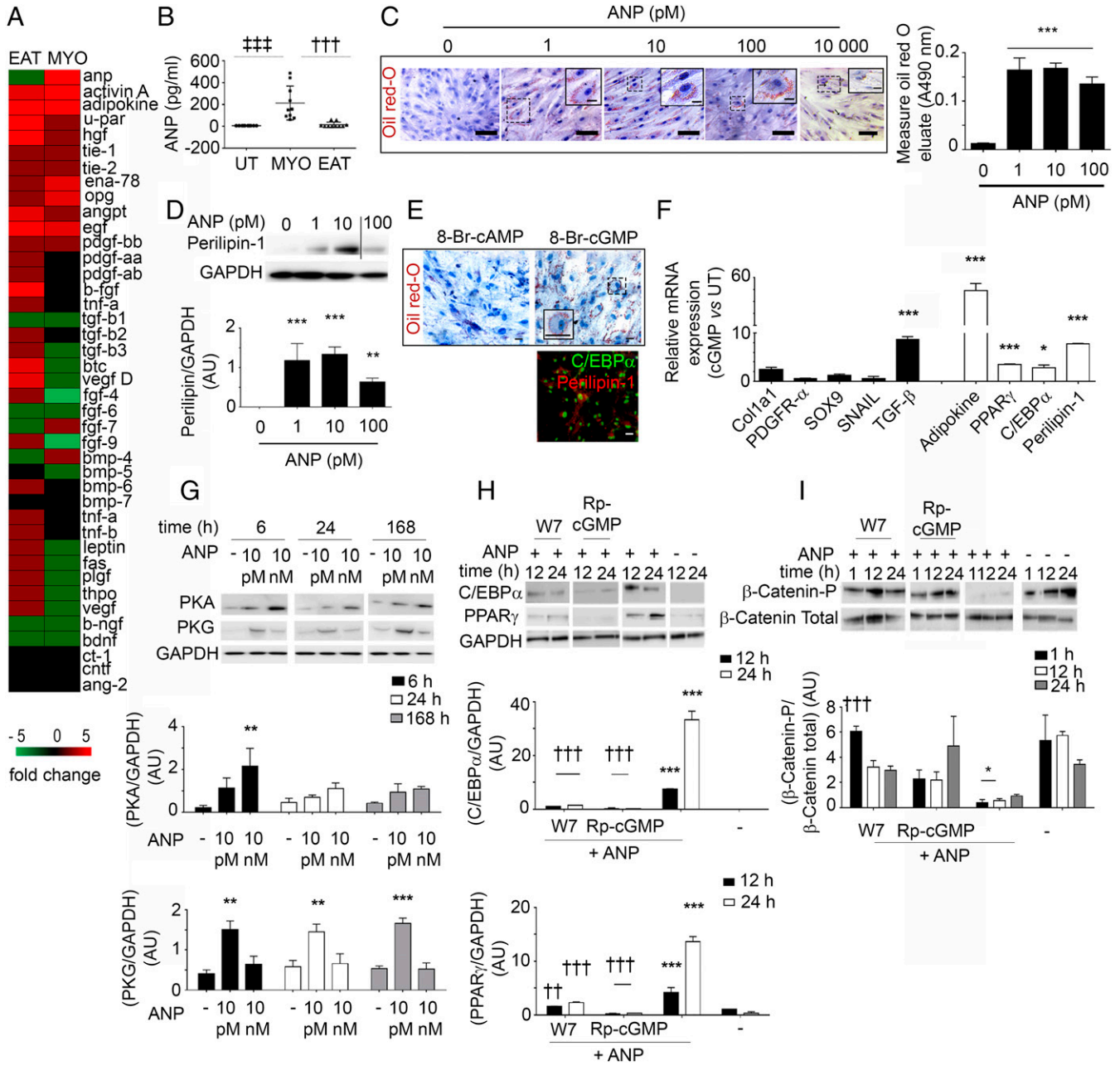


Fig. 5. The natriuretic peptide induces adipogenic differentiation of adult EPDCs. (*A*) Screening of proteins present in MYO-S ($n = 8$) or EAT-S ($n = 8$). (*B*) ANP levels in secretome measured by an ELISA assay (MYO-S, $n = 15$; EAT-S, $n = 10$). Data are expressed as mean ± SEM; $^{\dagger\dagger\dagger}P < 0.001$ compared with EAT-S; $^{\ddagger\ddagger\ddagger}P < 0.001$ compared with untreated (UT) cells, one-way ANOVA and Bonferroni's post hoc test. (*C*) Bright-field images of aEPDCs treated with ANP and stained with Oil Red O/hematoxylin ($n = 4$). (Scale bars: 20 μm; *Insets* 5 μm.) The histogram represents the Oil Red O content of the cultures (Oil Red O elution at A490 nm). Data are expressed as the mean ± SEM of independent experiments. $^{***}P < 0.001$ compared with untreated aEPDCs, one-way ANOVA and Bonferroni's post hoc test. (*D*) Immunoblot and relative quantification of Perilipin-1 vs. GAPDH expression in aEPDCs treated with ANP for 21 d ($n = 4$). Vertical line indicates splicing between blots. Data are expressed as the mean ± SEM of independent experiments. $^{**}P < 0.01$, $^{***}P < 0.001$ compared with untreated aEPDCs, one-way ANOVA and Bonferroni's post hoc test. (*E*) Oil Red O/hematoxylin staining and C/EBPα and Perilipin-1 immunostaining of aEPDCs treated with 8-Br-cGMP or 8-Br-cAMP ($n = 3$). (Scale bars: 20 μm; *Inset* 5 μm.) (*F*) qPCR analysis of adipogenic genes and mesenchymal transcripts from aEPDCs treated with 8-Br-cGMP for 21 d ($n = 4$). Data are presented as the fold change relative to untreated aEPDCs and are expressed as the mean ± SEM of independent experiments. $^{*}P < 0.05$, $^{***}P < 0.001$, one-way ANOVA and Bonferroni's post hoc test. (*G–I*) Immunoblots and relative quantification of PKA and PKG (*G*), C/EBPα and PPARγ (*H*), and β-catenin (*I*) expression in aEPDCs pretreated with W7 or Rp-GMPc (*H* and *I*) and treated with ANP (*G–I*). Data are expressed as the mean ± SEM of independent experiments. $^{*}P < 0.05$, $^{**}P < 0.01$, $^{***}P < 0.001$ compared with untreated aEPDCs. $^{\dagger\dagger}P < 0.01$, $^{\dagger\dagger\dagger}P < 0.001$ compared with aEPDCs treated with ANP, one-way ANOVA and Bonferroni's post hoc test.

addition to their classical expression in atrial adipocytes and myocytes, NPRA and NPRC also were detected in aEPDCs in the subepicardium of human atrial sections (Fig. 6*A*). Of note, a subset of Pref-1^{+} cells coexpressing NPRA was detected in the epicardial layer and also in the subepicardium (Fig. 6*B*). Furthermore, NPRA was expressed in aEPDCs in vitro at both the mRNA and protein levels (Fig. 6 *C–E*).

The involvement of NPRA in the adipogenic effect of ANP on aEPDCs was studied using a specific NPRA antagonist, HS-8140 (34, 35). After 21 d of incubation, HS-8140 decreased PPARγ and

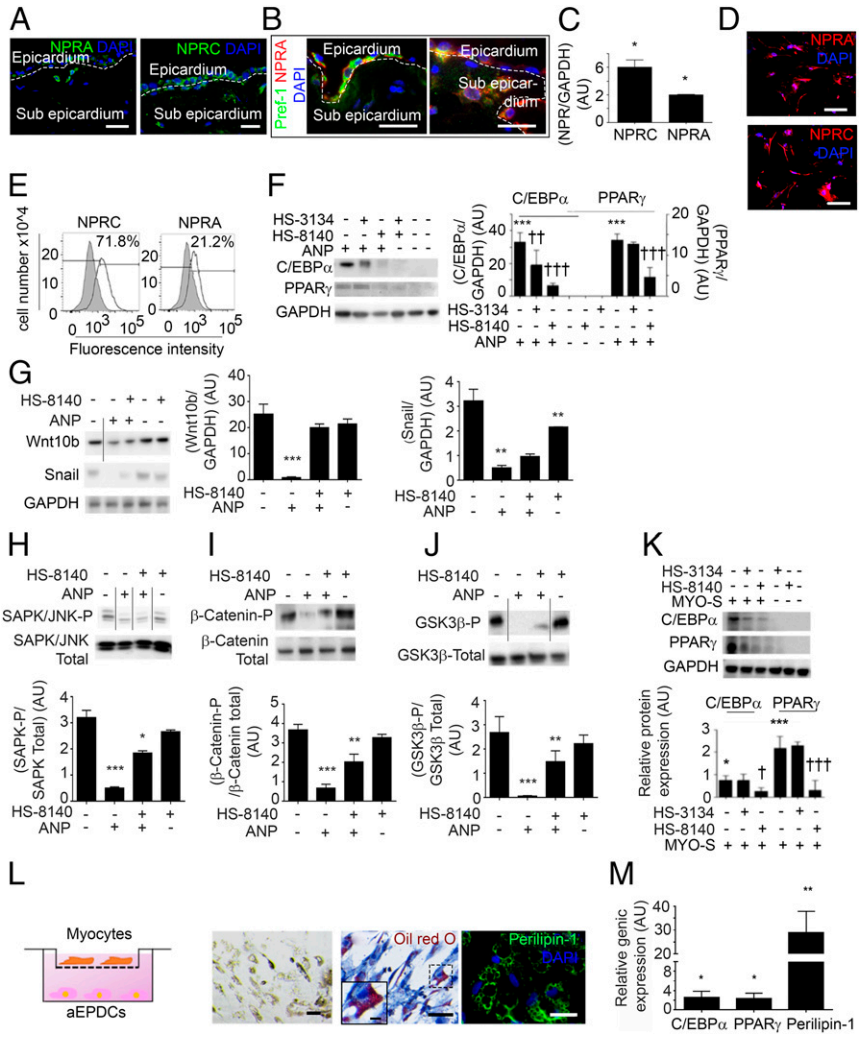


Fig. 6. The NPRA type receptor is involved in the adipogenic effect of ANP. (*A* and *B*) Immunofluorescence staining for NPRA, NPRC (*A*) and costaining for Pref-1 and NPRA (*B*) in 7-μm-thick sections of human atrial tissue ($n = 6$). (Scale bars, 10 μm.) (*C*) NPRA and NPRC expression in aEPDCs analyzed by Western blot ($n = 3$). Data are expressed as the mean ± SEM of three independent experiments. $^{*}P < 0.05$, unpaired *t* test. (*D*) Adult EPDCs expression for NPRA and NPRC analyzed by immunofluorescence ($n = 4$) (Scale bars, 20 μm.) (*E*) Expression for NPRA and NPRC analyzed by flow cytometry in aEPDCs ($n = 5$). (*F* and *K*) aEPDCs pretreated with NPRA antagonist (HS-8140) or NPRC antagonist (HS-3134) and then treated with ANP (*F*) ($n = 3$) or MYO-S (*K*) ($n = 3$) for 21 d were assessed by immunoblots. Relative quantification for C/EBPα and PPARγ is compared with untreated cells (*F* and *K*) (mean ± SEM of independent experiments $^{*}P < 0.05$; $^{***}P < 0.001$; $^{\dagger\dagger}P < 0.01$, $^{\dagger\dagger\dagger}P < 0.001$ compared with human EPDCs treated with ANP (*F*) or MYO-S (*K*); one-way ANOVA and Bonferroni's post hoc test). (*G–J*) aEPDCs pretreated with NPRA antagonist (HS-8140) ($n = 3$) and treated with ANP ($n = 3$) for 21 d were assessed by immunoblots. Relative quantification of Wnt10b and Snail (*G*), SAPK/JNK (*H*), β-Catenin (*I*), and GSK3β (*J*) are compared with untreated cells (mean ± SEM of independent experiments; $^{*}P < 0.05$; $^{**}P < 0.01$; $^{***}P < 0.001$; one-way ANOVA and Bonferroni's post hoc test). Vertical lines indicates splicing between blots. (*L*, *Left*) Diagram representing the Transwell system. (*Right*) Oil Red O/hematoxylin staining and Perilipin-1 immunostaining of aEPDC cocultured with myocytes ($n = 3$). (Scale bars: 20 μm; *Inset* 5 μm.) (*M*) qPCR analysis of C/EBPα, PPARγ, and Perilipin-1 expression in aEPDCs ($n = 4$) cocultured with myocytes ($n = 3$) for 7 d. qPCR data are presented as the fold change relative to aEPDCs cultured without myocytes. Data are expressed as the mean ± SEM of independent experiments. $^{*}P < 0.05$, $^{**}P < 0.01$, compared with human EPDCs in normal culture; one-way ANOVA and Bonferroni's post hoc test.

C/EBPα expression in human aEPDCs treated with ANP (Fig. 6*F*). Conversely, NPRC inhibition by HS-3134 had no effect on aEPDC differentiation (Fig. 6*F*). The inhibition of NPRA by HS-8140 under ANP stimulation was associated with the maintained expression of Snail and Wnt10b, indicating the repression of adipogenesis (Fig. 6*G*) (16, 36). These results were in agreement with the persistence of SAPK/JNK and β-catenin/GSK-3β pathway activation in ANP-induced aEPDCs treated with HS-8140 (Fig. 6 *H–J*). In MYO-S culture conditions, HS-8140 repressed aEPDC, C/EBPα, and PPARγ expression (Fig. 6*K*). Taken together these results indicate that the ANP/NPRA axis regulates the differentiation of aEPDCs into adipocytes.

Atrial myocytes are the source of ANP in the adult heart and secrete ANP when maintained in primary culture (37, 38). Therefore, to establish the involvement of ANP in the adipogenic effect of atrial secretome further, isolated human atrial myocytes were maintained in primary culture conditions and plated on the upper chamber of Transwell dishes to induce adipogenic differentiation of confluent aEPDCs in the lower chamber (Fig. 6*L*). Indeed, after 7-d culture in the presence of human atrial myocytes, aEPDCs displayed an adipocyte phenotype, with the accumulation of lipid droplets stained by Oil Red O and Perilipin-1 expression (Fig. 6*L*) and the up-regulation of adipogenic genes *C/EBPα*, *PPARγ*, and *Perilipin-1* (Fig. 6*M*).

Discussion

EAT is now considered an important determinant of the progression of the substrate of AF (21). Here we showed that the atrial epicardium is a source of adipocytes that can contribute to the accumulation of EAT in adult atria and that myocardial ANP is a trigger of this process.

The capacity of epicardial cells to undergo EMT, to migrate, and to differentiate into smooth muscle cells or myofibroblasts is well established (7, 9, 20, 39), but their adipogenic potential in adults has remained controversial (9). In the present study we found that human and mouse adult EPDCs show a strong potential to differentiate into adipocytes in vitro. Moreover, both in human atria and in a murine genetic lineage tracing model, we provide evidence that adult atrial epicardial cells undergo EMT and differentiate into adipocytes. A similar phenomenon of mesenchymal transformation and adipogenic differentiation of epicardial progenitors has been reported in the atrioventricular canal during embryonic development (11, 40). Of note, the endocardium has been shown to contribute to cardiac adipocytes during development, but adult endocardial-to-fat transition has not yet been reported (41).

The precise contribution of de novo EMT of epicardial progenitors at the adult stage to EAT expansion is difficult to evaluate. Additional mechanisms could be the recruitment of developmentally derived undifferentiated mesenchymal cells (EPDCs) maintained in a latent state in subepicardial layer (42). Resident and committed adipocyte progenitor cells in the atrial epicardial layer also could participate in EAT expansion. Indeed, $WT1^+$ mesothelial cells originating in the lateral plate mesoderm can give rise to several visceral fat depots as well as to the epicardium and sup-epicardial adipocytes (12, 40). These early mesodermal $WT1^+$ cells, although contributing to adipogenesis, could not be labeled by the tomato in our experiments, the recombinase being induced at the adult stage. Interestingly, we found strong and specific expression of $WT1^+$/Pref-1^+ in most epicardial cells during development as early as embryonic day (E)12.5. In particular, Pref-1 expression was high in atrial epicardial cells before and following epicardial EMT, suggesting that the atrial epicardium has adipogenic potential throughout cardiac development. The observation of $WT1^+$ cells in both sup- and subepicardial AT suggests that both fat depots have a common cellular origin. However, the mechanisms regulating their respective expansion might be distinct; for instance, subepicardial fat infiltration could require chemotactic factors to drive the migration of epicardial progenitors. We found that the adipogenic capacity of aEPDCs varies among patients and could depend on clinical conditions such as aging, left ventricular dysfunction, or AF. This variation is in agreement with the current idea that adipose depots are a common component of the atrial myocardium that could regulate the metabolic or oxidative status of neighboring myocardium. However, various clinical factors could regulate its expansion (6, 43). Under various AF-associated clinical conditions, this adipose depot can become deleterious, e.g., can favor myocardial fibrosis and the development of AF substrate (43).

We found that the secretome of atrial myocardium is a potent inducer of epicardial cell adipogenesis by activating key kinases reported to regulate adipocyte formation (19, 22, 23, 36). This activation is supported by the observation that the atrial secretome suppressed the mesenchymal signaling pathways Wnt/β-catenin/GSK-3β (19, 36) and SAPK/JNK MAPK (22, 23), whereas it stimulated ERK/MAPK and PI3K/AKT which regulate the two adipogenic transcription factors C/EBPα and PPARγ. The effect of the atrial secretome is mediated primarily by ANP; other potential adipogenic factors secreted by the myocardium such FGF-7 and BMP-4 did not induce adipogenic differentiation of aEPDCs. The natriuretic peptide binds to the NPRA receptor, activating cGMP-dependent signaling pathways and the recruitment of the transcriptional adipogenic factors PPARγ and C/EBPα. PDE enzymes that regulate the balance between intracellular cGMP and cAMP levels are involved in the adipogenic effect of ANP, as indicated by the down-regulation of C/EBPα and PPARγ expression and the maintenance of a mesenchymal state of aEPDCs incubated with a PDE inhibitor. Distinct PDE enzymes such as PDE3, PDE5, and PDE11 have been reported to be involved in the transition from pre- to mature adipocytes (44). Previous studies, mainly conducted with 3T3-L1 preadipocyte cell lines, have reported that cGMP-dependent signaling can regulate adipogenesis (45, 46). These studies notably reported activation of guanylyl cyclase-B by C-type natriuretic peptide or the inhibition of PDEs using 3-isobutyl-1-methylxanthine (IBMX) (45, 46). Furthermore, during embryonic development, the regulation by the NPRA/cGMP signaling pathway of the balance between proliferation and differentiation of cardiac progenitor cells is essential for cardiac growth (47). Therefore, the NPRA/cGMP signaling pathway appears to be a critical regulatory node for the effect of ANP on cardiac tissue homeostasis.

The adipogenic effect of ANP was observed after prolonged incubation of aEPDCs with a low peptide concentration, whereas the lipolytic effect was observed at a high peptide concentration and following short exposure. This observation suggests that adipogenic versus lipolytic effects could depend on the route of ANP secretion. Indeed, there is a regulated secretory pathway for ANP that is activated in response to atrial stretch and which results in the transient release of mature peptides stored in intracellular granules. There also is a constitutive pathway, without intervening secretion stimuli, in which the hormone is secreted after synthesis (48, 49), as observed in hypertrophied myocardium (50). During permanent AF characterized by a certain degree of myocardial hypertrophy, constitutive release of ANP is activated, resulting in local accumulation of the peptide; this local accumulation could favor the adipogenic effects of ANP and in turn the expansion of EAT, as observed in this clinical setting (51).

Natriuretic peptides are known to regulate AT metabolism in a dose-dependent manner (52, 53). Acutely, they can stimulate human fat cell lipolysis through PKG (30, 54) and were shown more recently to turn on the expression of the thermogenic machinery toward the browning of white adipocytes (55). Our present data identify a further role for natriuretic peptides in epicardial fat formation, indicating that these molecules could regulate a continuum from the recruitment of fat cell progenitors to their functional role in the release of fatty acids. In addition to natriuretic peptides, other factors produced in different pathological contexts could drive the transition of epicardium progenitors to fat. For instance, IGF1R could induce the aEPDCs-derived adipocytes following myocardial infarction (12). Moreover, rapid atrial beating in pigs and permanent AF in humans are associated with the expression of several genes able to regulate AT accumulation in human and pig atrial myocardium, a phenomenon attributed to an insufficient supply of oxygen and nutriments (11). Another example of cross-talk between AT and the atrial myocardium comes from the observation that human EAT secretes adipokines that regulate the oxidative status of the atrial myocardium (56). EAT expansion also could be caused by nutrient excess in which epicardium becomes engorged with lipids resulting from the overwhelmed capacity of s.c. AT to clear excess triglycerides. This possibility is indicated by our observation that in mice, sustained HFD pressure is necessary to reveal fat accumulation in the atria, whereas massive adipose infiltration of the posterior wall of left atria is easily described in sheep with moderate obesity (57).

In summary, we show that adult atrial epicardium-to-fat transition contributes to atrial EAT, and we provide evidence that this process is driven by ANP secreted by the myocardium. Our results support the idea that EAT accumulation in adult atria is a slow process that could occur in response to chronic alterations of atrial myocardium workload and metabolic conditions. Cardiac AT is a source of free fatty acids, the preferred metabolic substrates of cardiomyocytes, and its accumulation in diseased atrial myocardium could be part of an adaptive process. However, the downside of this process is the risk of progression of the substrate of AF because of the role played by EAT in atrial fibrosis (5, 6).

Therefore, the epicardium-to-fat transition could be an early step in the formation of the substrate of AF.

Methods

Study Approval. All animal experiments conform to the Guide for the Care and Use of Laboratory Animals, according to Directive 2010/63/EU of the European Parliament and were approved by the local committee of animal care (agreement A751315).

Human tissue samples were obtained from patients undergoing cardiovascular surgery as a bridge or for valvulopathy. Data and samples were obtained in accordance with French Law Huriet-Sérusclat and with the approval of the Ethical Committee (Comité de Protection des Personne Ile-de France VI) of Pitié-Salpêtrière Hospital, and informed consent to the research was obtained from each patient. The use of personal treatment data necessary for the research was reported to the National Commission for Data Protection and Liberties (CNIL-France) under the Data Protection Act number 78-17.

Mice. Eight-week-old male mice were used for all mouse studies and were maintained under a 12-h light/12-h dark cycle at constant temperature (23 °C) with free access to food and water. $WT1^{CreERT2+/-}$ and $Rosa26^{tdTomato+/+}$ mice on a C57BL/6J background were purchased from Jackson Laboratories. $WT1^{CreERT2+/-}$ mice were bred with $Rosa26^{tdT+/+}$ mice. To trace the lineage and follow $WT1^{+}$ epicardial progenitors, the male offspring were injected with tamoxifen to induce the recombinase at the adult stage (5 wk) as previously described (58). $WT1^{CreERT2+/-}Rosa^{tdT+/-}$ transgenic mice (n = 10) and C57BL/6J wild-type mice (n = 30) (23–28 g; purchased from Janvier Laboratories-CERJ) were fed an HFD (60% fat) (D12492i; Research Diets, Inc.) (n = 20) or a normal diet (4% fat) (n = 20) for 4 mo. The hearts were removed, perfused through the aorta with PBS, fixed in 4% (wt/vol) paraformaldehyde (PFA) overnight, dehydrated overnight in 7, 14, and 25% (wt/vol) sucrose, embedded in Optimum Cutting Temperature (O.C.T.) compound, frozen, and sectioned (7 μm).

Human Tissue. Appendage samples of human atrial tissue were obtained for secretome study (n = 29), histological study (n = 26), and isolation of epicardial progenitor cells (n = 35). Samples of epicardial fat tissue (n = 22) were dedicated for secretome study. The subjects' clinical data are provided in Table S1.

Masson's Trichrome Staining. Human atrial appendage samples (n = 26) were fixed and embedded in paraffin as previously described (6). Frozen 7-μm-thick sections of mouse atria or 7-μm-thick paraffin-embedded sections of human atria (n = 26) were stained with Masson's trichrome according to the manufacturer's instructions (Sigma-Aldrich). Images were acquired with a Nikon DS-Ri1 camera coupled to an Eclipse-Ti Nikon microscope and Nis-Element software (Nikon France S.A.) and were analyzed with Image J software.

Human Secretomes. Human atrial tissue (MYO) (n = 29) or EAT (n = 22) was placed at 37 °C, 5% CO_2, in DMEM supplemented with 1% penicillin-streptomycin. After 24 h, conditioned medium (secretome, -S) was removed and conserved at −80 °C. The subjects' clinical data are provided in Table S1.

Protein Screening Assay. Human atrial tissue secretome (MYO-S) (n = 8), EAT secretome (EAT-S) (n = 5), or aEDPC-derived adipocyte supernatant (n = 4) was screened with a cytokine array (catalog no. 126-AAH-CYT-2000-4; Tebu-Bio) and an Adipokine array (R&D Systems) according to the manufacturers' instructions. ELISA of the ANP level was performed in EAT-S (n = 22) or MYO-S (n = 29) according to the manufacturer's instructions (R&D Systems).

Ex Vivo Culture of aEPDCs. Stripped layers of atrial epicardium were first incubated in six-well plates for 2 d in DMEM (Thermo Fisher Scientific) supplemented with 10% (vol/vol) FCS and 1% penicillin-streptomycin (Sigma-Aldrich). After spontaneous migration of aEPDCs, tissue was removed, and cells were cultured in 1:1 DMEM and M199 medium (Thermo Fisher Scientific) supplemented with 10% (vol/vol) FCS, 1% penicillin-streptomycin, and basic FGF (bFGF) (10 ng/mL) at 37 °C, 5% CO_2. The medium was changed every 2 d. Subjects' clinical data are provided in Table S1.

Human MSCs. Adipose-derived stem cells (R7788-115) from human AT were isolated and cultured according to the manufacturer's instructions (Thermo Fisher Scientific).

Isolation of Human Myocytes. Myocyte isolation and culture from human atrial tissue were performed as previously described (59). Briefly, cell dissociation was achieved by enzymatic steps using collagenase (type IV) and protease (type XXIV) (Sigma-Aldrich). Isolated myocytes were cultured in DMEM (Thermo Fisher Scientific) supplemented with 10% (vol/vol) FCS (Sigma-Aldrich), nonessential amino acids, 1 nM insulin, and antibiotics (100 IU/mL penicillin and 0.1 μg/mL streptomycin) (Thermo Fisher Scientific). To inhibit fibroblast proliferation, 10 μM cytosine β-D-arabinofuranoside (Sigma-Aldrich) was added to the myocyte culture. After 7 d in these culture conditions, human atrial myocytes underwent a marked growth and dedifferentiation process, as previously characterized (59).

Coculture Assay. Human aEPDCs were cultured at a density of 1.10^6 cells/mL in the lower chamber of a six-plate Transwell system, and myocytes were incubated at a final density of 50×10^3/mL in the upper, laminin-coated (10 μg/mL) (Thermo Fisher Scientific) chamber (Verfilco). Coculture was maintained for 7 d at 37 °C, 5% CO_2. The medium was changed once each week.

Differentiation of aEPDCs. Human or $WT1^{CreERT2+/-}Rosa^{tdT+/-}$ transgenic mouse aEPDCs were incubated in adipogenic basal medium composed of DMEM/F12 (Invitrogen) supplemented with insulin (5 μg/mL), ascorbic acid (200 μM), 10% (vol/vol) FCS (Sigma-Aldrich), bicarbonate (14 mM), and 1% penicillin-streptomycin (Thermo Fisher Scientific). To induce adipocyte differentiation, the adipogenic basal medium was supplemented with MYO-S (1/100), ANP (1, 10, 100 pM or 10 nM) (Sigma-Aldrich), 8-Br-cGMP (10 nM) (Sigma-Aldrich), 8-Br-cAMP (10 nM) (Sigma-Aldrich), FGF-7 (10 μM) (Sigma-Aldrich), or BMP-4 (50 ng/mL) (Sigma-Aldrich) for 7 or 21 d. Two positive controls were used. The first was adipogenic medium 1 composed of adipogenic basal medium supplemented with biotin (8 μM), dexamethasone (1 μM) (Sigma-Aldrich), 3,3′,5-triiodo-l-thyronine (T3) (1 nM) (Sigma-Aldrich), and IBMX (500 μM) (Sigma-Aldrich) for 21 d (21, 60). The second control was adipogenic medium 2 in which aEPDCs were cultured according to the manufacturer's instructions (Thermo Fisher Scientific). All media were changed twice each week.

Oil Red Staining. MSCs (n = 3) or aEPDC-derived adipocytes (n = 31) were fixed with 4% (wt/vol) PFA, incubated with 60% (vol/vol) isopropanol, and stained with 3% (vol/vol) Oil Red O (Sigma-Aldrich). Then the cell nuclei were counterstained with hematoxylin (Sigma-Aldrich). Oil-red O staining then was eluted with isopropanol and quantified using spectrophotometry at 492 nm. All images were acquired with a Nikon DS-Ri1 camera coupled to an Eclipse-Ti Nikon microscope and Nis-Element software (Nikon France S.A.) and were analyzed with Image J software.

Statistics. Data are expressed as means ± SEM. Differences were investigated using the appropriate t test or one-way ANOVA and a Bonferroni post hoc analysis and were considered significant at $P < 0.05$. Statistical analysis was performed with GraphPad Prism 6.0 (GraphPad Software, Inc.).

ACKNOWLEDGMENTS. We thank the Leducq Foundation for its continuous support of our research. This work was supported by the French National Agency through the national program Investissements d'Avenir Grant ANR-10-IAHU-05 (to N.S., M.F., K.C., and S.N.H.) and though the Recherche Hospital-Universitaire-Cardiac & Skeletal Muscle Alteration in Relation to Metabolic Diseases and Ageing: Role of Adipose Tissue (RHU-CARMMA) Grant ANR-15-RHUS-0003 and the Fondation de La Recherche Medicale (to N.S., T.M.-M., M.P., and S.N.H.). This project received funding from the European Union's Horizon 2020 Research and Innovation Programme under Grant 633193 "CATCH ME" and from Fondation Leducq "Structural Alterations in the Myocardium and the Substrate for Cardiac Fibrillation" (N.S. and S.N.H.). N.S. was supported by European Union Program Horizon 2020 (CATCH ME). T.M.-M. was supported by the Leducq Foundation (SHAPEHEART) and the William Harvey International Translational Research Academy European Union COFUND Program.

1. Iacobellis G (2015) Local and systemic effects of the multifaceted epicardial adipose tissue depot. *Nat Rev Endocrinol* 11(6):363–371.
2. Al Chekakie MO, et al. (2010) Pericardial fat is independently associated with human atrial fibrillation. *J Am Coll Cardiol* 56(10):784–788.
3. Thanassoulis G, et al. (2010) Pericardial fat is associated with prevalent atrial fibrillation: The Framingham Heart Study. *Circ Arrhythm Electrophysiol* 3(4):345–350.
4. Wong CX, et al. (2011) Pericardial fat is associated with atrial fibrillation severity and ablation outcome. *J Am Coll Cardiol* 57(17):1745–1751.
5. Venteclef N, et al. (2015) Human epicardial adipose tissue induces fibrosis of the atrial myocardium through the secretion of adipo-fibrokines. *Eur Heart J* 36(13):795a–805a.
6. Haemers P, et al. (2015) Atrial fibrillation is associated with the fibrotic remodelling of adipose tissue in the subepicardium of human and sheep atria. *Eur Heart J* ehv625 10.1093/eurheartj/ehv625.
7. Chong JJH, et al. (2011) Adult cardiac-resident MSC-like stem cells with a proepicardial origin. *Cell Stem Cell* 9(6):527–540.

8. Bollini S, et al. (2014) Re-activated adult epicardial progenitor cells are a heterogeneous population molecularly distinct from their embryonic counterparts. *Stem Cells Dev* 23(15):1719–1730.
9. van Tuyn J, et al. (2007) Epicardial cells of human adults can undergo an epithelial-to-mesenchymal transition and obtain characteristics of smooth muscle cells in vitro. *Stem Cells* 25(2):271–278.
10. Yamaguchi Y, et al. (2015) Adipogenesis and epicardial adipose tissue: A novel fate of the epicardium induced by mesenchymal transformation and PPARγ activation. *Proc Natl Acad Sci USA* 112(7):2070–2075.
11. Liu Q, et al. (2014) Epicardium-to-fat transition in injured heart. *Cell Res* 24(11): 1367–1369.
12. Zangi L, et al. (2016) An IGF1R-dependent pathway drives epicardial adipose tissue formation after myocardial injury. *Circulation* CIRCULATIONAHA.116.022064 10.1161/CIRCULATIONAHA.116.022064.
13. Sun Y, et al. (2007) Islet 1 is expressed in distinct cardiovascular lineages, including pacemaker and coronary vascular cells. *Dev Biol* 304(1):286–296.
14. Zhou B, et al. (2008) Epicardial progenitors contribute to the cardiomyocyte lineage in the developing heart. *Nature* 454(7200):109–113.
15. Singh MK, Epstein JA (2012) Epicardium-derived cardiac mesenchymal stem cells: Expanding the outer limit of heart repair. *Circ Res* 110(7):904–906.
16. Lee YH, et al. (2013) Transcription factor Snail is a novel regulator of adipocyte differentiation via inhibiting the expression of peroxisome proliferator-activated receptor γ. *Cell Mol Life Sci* 70(20):3959–3971.
17. Pittenger MF, et al. (1999) Multilineage potential of adult human mesenchymal stem cells. *Science* 284(5411):143–147.
18. Jiang C, et al. (2015) HIF-1A and C/EBPs transcriptionally regulate adipogenic differentiation of bone marrow-derived MSCs in hypoxia. *Stem Cell Res Ther* 6:21.
19. Tang Q-Q, et al. (2005) Sequential phosphorylation of CCAAT enhancer-binding protein beta by MAPK and glycogen synthase kinase 3beta is required for adipogenesis. *Proc Natl Acad Sci USA* 102(28):9766–9771.
20. Asli NS, Xaymardan M, Harvey RP (2014) Epicardial origin of resident mesenchymal stem cells in the adult mammalian heart. *J Dev Biol* 2(2):117–137.
21. Chilukoti RK, et al. (2015) Atrial fibrillation and rapid acute pacing regulate adipocyte/adipositas-related gene expression in the atria. *Int J Cardiol* 187:604–613.
22. Bost F, Aouadi M, Caron L, Binétruy B (2005) The role of MAPKs in adipocyte differentiation and obesity. *Biochimie* 87(1):51–56.
23. Prusty D, Park B-H, Davis KE, Farmer SR (2002) Activation of MEK/ERK signaling promotes adipogenesis by enhancing peroxisome proliferator-activated receptor gamma (PPARgamma) and C/EBPalpha gene expression during the differentiation of 3T3-L1 preadipocytes. *J Biol Chem* 277(48):46226–46232.
24. Zhang T, Guan H, Yang K (2010) Keratinocyte growth factor promotes preadipocyte proliferation via an autocrine mechanism. *J Cell Biochem* 109(4):737–746.
25. Tsukamoto O, et al. (2009) Natriuretic peptides enhance the production of adiponectin in human adipocytes and in patients with chronic heart failure. *J Am Coll Cardiol* 53(22):2070–2077.
26. Souza SC, et al. (2011) Atrial natriuretic peptide regulates lipid mobilization and oxygen consumption in human adipocytes by activating AMPK. *Biochem Biophys Res Commun* 410(3):398–403.
27. Pisani DF, et al. (2015) Visfatin expression analysis in association with recruitment and activation of human and rodent brown and brite adipocytes. *Adipocyte* 5(2):186–195.
28. Liangpunsakul S, et al. (2014) Increasing serum pre-adipocyte factor-1 (Pref-1) correlates with decreased body fat, increased free fatty acids, and level of recent alcohol consumption in excessive alcohol drinkers. *Alcohol* 48(8):795–800.
29. Zhang X, et al. (2010) Sildenafil promotes adipogenesis through a PKG pathway. *Biochem Biophys Res Commun* 396(4):1054–1059.
30. Moro C, Klimcakova E, Lafontan M, Berlan M, Galitzky J (2007) Phosphodiesterase-5A and neutral endopeptidase activities in human adipocytes do not control atrial natriuretic peptide-mediated lipolysis. *Br J Pharmacol* 152(7):1102–1110.
31. Ikoma-Seki K, et al. (2015) Role of LRP1 and ERK and cAMP signaling pathways in lactoferrin-induced lipolysis in mature rat adipocytes. *PLoS One* 10(10):e0141378.
32. Hemmrich K, et al. (2010) Nitric oxide and downstream second messenger cGMP and cAMP enhance adipogenesis in primary human preadipocytes. *Cytotherapy* 12(4): 547–553.
33. Pandey KN (2014) Guanylyl cyclase/natriuretic peptide receptor-A signaling antagonizes phosphoinositide hydrolysis, Ca(2+) release, and activation of protein kinase C. *Front Mol Neurosci* 7:75.
34. Moro C, et al. (2004) Functional and pharmacological characterization of the natriuretic peptide-dependent lipolytic pathway in human fat cells. *J Pharmacol Exp Ther* 308(3):984–992.
35. Houshmand F, Faghihi M, Zahediasl S (2015) Role of atrial natriuretic Peptide in oxytocin induced cardioprotection. *Heart Lung Circ* 24(1):86–93.
36. Ross SE, et al. (2000) Inhibition of adipogenesis by Wnt signaling. *Science* 289(5481): 950–953.
37. Dietz JR (2005) Mechanisms of atrial natriuretic peptide secretion from the atrium. *Cardiovasc Res* 68(1):8–17.
38. de Bold AJ, de Bold MLK (2005) Determinants of natriuretic peptide production by the heart: Basic and clinical implications. *J Investig Med* 53(7):371–377.
39. Zhou B, et al. (2011) Adult mouse epicardium modulates myocardial injury by secreting paracrine factors. *J Clin Invest* 121(5):1894–1904.
40. Chau Y-Y, et al. (2014) Visceral and subcutaneous fat have different origins and evidence supports a mesothelial source. *Nat Cell Biol* 16(4):367–375.
41. Zhang H, et al. (2016) Endocardium contributes to cardiac fat. *Circ Res* 118(2):254–265.
42. Ruiz-Villalba A, Ziogas A, Ehrbar M, Pérez-Pomares JM (2013) Characterization of epicardial-derived cardiac interstitial cells: Differentiation and mobilization of heart fibroblast progenitors. *PLoS One* 8(1):e53694.
43. Hatem SN, Sanders P (2014) Epicardial adipose tissue and atrial fibrillation. *Cardiovasc Res* 102(2):205–213.
44. Armani A, Marzolla V, Rosano GMC, Fabbri A, Caprio M (2011) Phosphodiesterase type 5 (PDE5) in the adipocyte: A novel player in fat metabolism? *Trends Endocrinol Metab* 22(10):404–411.
45. Katafuchi T, Garbers DL, Albanesi JP (2010) CNP/GC-B system: A new regulator of adipogenesis. *Peptides* 31(10):1906–1911.
46. Mitschke MM, et al. (2013) Increased cGMP promotes healthy expansion and browning of white adipose tissue. *FASEB J* 27(4):1621–1630.
47. Hotchkiss A, et al. (2015) Atrial natriuretic peptide inhibits cell cycle activity of embryonic cardiac progenitor cells via its NPRA receptor signaling axis. *Am J Physiol Cell Physiol* 308(7):C557–C569.
48. Thibault G, Amiri F, Garcia R (1999) Regulation of natriuretic peptide secretion by the heart. *Annu Rev Physiol* 61:193–217.
49. Ogawa T, Vatta M, Bruneau BG, de Bold AJ (1999) Characterization of natriuretic peptide production by adult heart atria. *Am J Physiol* 276(6 Pt 2):H1977–H1986.
50. Ruskoaho H, Vakkuri O, Arjamaa O, Vuolteenaho O, Leppäluoto J (1989) Pressor hormones regulate atrial-stretch-induced release of atrial natriuretic peptide in the pithed rat. *Circ Res* 64(3):482–492.
51. Roy D, et al. (1987) Atrial natriuretic factor during atrial fibrillation and supraventricular tachycardia. *J Am Coll Cardiol* 9(3):509–514.
52. Nishikimi T, et al. (2009) Stimulatory and Inhibitory regulation of lipolysis by the NPR-A/cGMP/PKG and NPR-C/G(i) pathways in rat cultured adipocytes. *Regul Pept* 153(1-3): 56–63.
53. Lafontan M, et al. (2008) Control of lipolysis by natriuretic peptides and cyclic GMP. *Trends Endocrinol Metab* 19(4):130–137.
54. Sengenès C, Berlan M, De Glisezinski I, Lafontan M, Galitzky J (2000) Natriuretic peptides: A new lipolytic pathway in human adipocytes. *FASEB J* 14(10):1345–1351.
55. Bordicchia M, et al. (2012) Cardiac natriuretic peptides act via p38 MAPK to induce the brown fat thermogenic program in mouse and human adipocytes. *J Clin Invest* 122(3):1022–1036.
56. Antonopoulos AS, et al. (2016) Mutual regulation of epicardial adipose tissue and myocardial redox state by PPAR-γ/adiponectin signalling. *Circ Res* 118(5):842–855.
57. Mahajan R, et al. (2015) Electrophysiological, electroanatomical, and structural remodeling of the atria as consequences of sustained obesity. *J Am Coll Cardiol* 66(1): 1–11.
58. Moore-Morris T, et al. (2014) Resident fibroblast lineages mediate pressure overload-induced cardiac fibrosis. *J Clin Invest* 124(7):2921–2934.
59. Rücker-Martin C, Pecker F, Godreau D, Hatem SN (2002) Dedifferentiation of atrial myocytes during atrial fibrillation: Role of fibroblast proliferation in vitro. *Cardiovasc Res* 55(1):38–52.
60. Elsen M, et al. (2014) BMP4 and BMP7 induce the white-to-brown transition of primary human adipose stem cells. *Am J Physiol Cell Physiol* 306(5): C431–C440.